ACSNANO

www.acsnano.org

ARTICLE

# Vertically Aligned Graphene Sheets Membrane for Highly Efficient Solar Thermal Generation of Clean Water

Panpan Zhang, Jing Li, Lingxiao Lv, Yang Zhao, and Liangti Qu*

Beijing Key Laboratory of Photoelectronic/Electrophotonic Conversion Materials, Key Laboratory of Cluster Science, Ministry of Education, School of Chemistry, Beijing Institute of Technology, Beijng 100081, P. R. China

Supporting Information

**ABSTRACT:** **Efficient utilization of solar energy for clean water is an attractive, renewable, and environment friendly way to solve the long-standing water crisis. For this task, we prepared the long-range vertically aligned graphene sheets membrane (VA-GSM) as the highly efficient solar thermal converter for generation of clean water. The VA-GSM was prepared by the antifreeze-assisted freezing technique we developed, which possessed the run-through channels facilitating the water transport, high light absorption capacity for excellent photothermal transduction, and the extraordinary stability in rigorous conditions. As a result, VA-GSM has achieved average water evaporation rates of 1.62 and 6.25 kg $m^{-2}$ $h^{-1}$ under 1 and 4 sun illumination with a superb solar thermal conversion efficiency of up to 86.5% and 94.2%, respectively, better than that of most carbon materials reported previously, which can efficiently produce the clean water from seawater, common wastewater, and even concentrated acid and/or alkali solutions.**

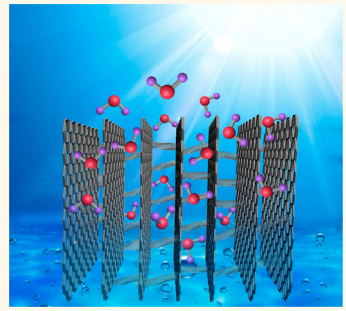

**KEYWORDS:** *vertically aligned graphene sheets membrane, graphene assembly, solar thermal conversion, steam generation, clean water*

With the fast development of modern industry, we are nowadays facing a more and more serious water pollution problem. Efficient utilization of solar energy to generate the clean water from seawater and even industrial wastewater is a promising approach to solve the shortage of water resources.[1−4] Solar desalination is currently the research hotspot for steam generation of water from seawater. Examples for photothermal conversion materials include three-dimensional (3D) nanoporous anodic aluminum oxide membranes assembled with aluminum nanoparticles,[5] polypyrrole-deposited stainless steel mesh,[6] airlaid-paper-based Au nanoparticle film,[7] and bilayered hybrid biofoam composed of bacterial nanocellulose and reduced graphene oxide (rGO).[8] However, for practical application, the photothermal conversion materials should be easily scaled up and stable in many of rigorous circumstances such as organic, strong caustic acid, and/or alkali conditions.

3D graphene-based materials with high porosity,[9−12] outstanding light absorption,[13] excellent photothermal transduction,[8,14] and stability in many extreme conditions (*e.g.*, ~3000 °C high temperature[15] and −196 °C low temperature),[16,17] strong acid and alkali survivability,[18,19] are one of the most attractive candidates for efficient solar thermal production of clean water. Herein, we demonstrated the scalable fabrication of vertically aligned graphene sheets membrane (VA-GSM) that meets the requirements expected for efficient solar thermal generation, such as vertically aligned channels for release of water vapor, $O_2$-plasma enhanced hydrophilic surfaces, high absorption in the full solar spectrum range (from 250 to 2500 nm) for excellent photothermal transduction. The efficiencies are up to 86.5% under 1 sun and 94.2% under 4 sun illumination, superior to most of the previous reports. Moreover, VA-GSM can not only generate the clean water from seawater but also work well in common wastewater and concentrated caustic acid and/or alkali solutions, promising for application in photothermal regeneration of clean water.

## RESULTS AND DISCUSSION

We have developed the antifreeze-assisted freezing technique for the large-scale preparation of long-range VA-GSM. In a typical synthesis process, GO suspension was mediated with a certain amount of ethanol (Figure 1a), which was transferred to a polytetrafluoroethylene (PTFE) mold placed on the surface of liquid nitrogen for freeze casting (Figure 1b). The as-obtained bulk was then treated with freeze-drying and thermal annealing (Figure 1c). The experimental details are included in the Experimental Section. Ethanol was specifically used as the antifreeze to decrease the freezing point, which has a pronounced effect on the crystallization behavior of ice growth, thus resulting in the well-organized assembly of graphene

Received: March 21, 2017
Accepted: April 19, 2017
Published: April 19, 2017

  

DOI: 10.1021/acsnano.7b01965
*ACS Nano* 2017, 11, 5087−5093

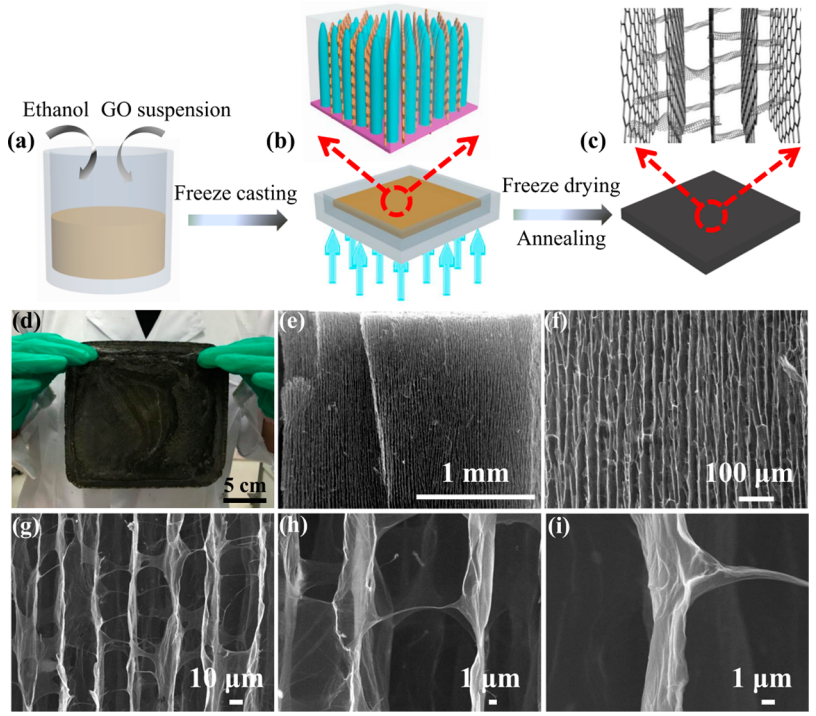


**Figure 1. Schematic of the fabrication process and characterization of VA-GSM. (a) GO suspension with a small amount of ethanol. (b) Directional freeze casting of GO mixture in a PTFE mold, which is placed on the surface of liquid nitrogen to induce the freezing direction from the bottom to top. (c) VA-GSM is obtained after freeze-drying and thermal annealing. (d) Photograph of monolith VA-GSM with a size of 16 cm × 16 cm. (e–i) SEM images of VA-GSM with different magnifications.**

sheets parallel to the ice axes.[20] After precisely controlling the freezing direction from the bottom to top, a 3D graphene membrane with vertically aligned graphene sheets was obtained. Vertically aligned assembly of graphene sheets was generally observed in the GO suspension containing ethanol, methanol, acetone, and *n*-propyl alcohol (Figure S1a–f), which is not the case in that of pyridine, cyclohexane, and acetic acid (Figure S1g–l). We provisionally proposed that the preferred adsorption of GO on curved ice crystal surface,[21] antifreeze-induced ice growth inhibition and directional freeze casting (Figure S2a–f) led to the formation of vertically aligned graphene sheets, although the detailed formation mechanism is still not clear. However, when compared with the marriage of graphene chemistry and ice physics for a monolithic structure reported preciously,[22] this antifreeze-assisted freezing technique developed here is really versatile and scalable for the production of a long-range vertically aligned graphene sheets membrane.

Figure 1d shows a VA-GSM with a size of 16 cm × 16 cm that possesses excellent mechanical properties, allowing to be bent (Figure S3a), cut (Movie S1), and compressed in large strain (Figure S3b,c). Scanning electron microscopy (SEM) of VA-GSM exhibits highly vertically aligned lamellar structures (Figures 1e and S4a,b), and the channel width is *ca.* 25–35 $\mu$m with a specific surface area of approximately 91 $m^2\ g^{-1}$ (Figures 1f and S4c,d). This structure is different than the cellular,[23,24] lamellar,[25] and onion-like[26] graphene networks reported previously. The enlarged view reveals the twisted and curled fibers bridging between the parallel graphene layers, probably coming from the rolling up of GO sheets during the cold quenching process (Figure 1g).[27,28] These built-in graphene bridges between vertical graphene layers make the VA-GSM stable enough for the self-supporting framework (Figure 1h,i). In fact, the formation of well-ordered skeletal structure is strongly dependent on the introduction of suitable amounts of ethanol (Figure S5).

The initially formed VA-GSM exhibits hydrophobic behavior with water contact angles (CA) of 120°. After $O_2$-plasma treatment, the hydrophilic surface is obtained with a CA of 0° (Figure S6a). The average water evaporation rates were measured to be 1.20 kg $m^{-2}$ $h^{-1}$ for hydrophobic counterpart, while it was 1.57 kg $m^{-2}$ $h^{-1}$ for hydrophilic VA-GSM and 0.51 kg $m^{-2}$ $h^{-1}$ for pure water under only 1 sun illumination (1 kW $m^{-2}$) (Figure S6b). Moreover, the average evaporation rate of pure water in dark environment is 0.24 kg $m^{-2}$ $h^{-1}$ (Figure S6b), which will be subtracted from all the measured evaporation rates to eliminate the effect of natural water evaporation. This hydrophilic feature improved the capillary effect for effective water infiltration (Figure S6c).[29] Under solar illumination of 1 sun, surface temperatures of VA-GSM in different thickness were carried out without contacting water. VA-GSM with the thickness of 2, 4, 6, and 8 mm have the similar surface temperatures, higher than that of VA-GSM with the thickness of 1 mm (Figure S7a). The VA-GSM with a thickness of 2 mm delivered the highest average water evaporation rate of 1.57 kg $m^{-2}$ (Figure S7b). The added thickness increases the transport distance of water during solar steam generation. Unless otherwise noted, we chose the VA-GSM with a thickness of 2 mm to conduct the experiments.

We investigated solar steam generation performance of VA-GSM with run-through channels compared with both rGO film and structure-disordered rGO foam (rGOF-DS) with the same weight, and all the samples have been treated with $O_2$-plasma to obtain the hydrophilic feature. The materials used for solar thermal steam generation may provide channels for fluid up to the surface, followed by forming steam at the air/water interface under solar illumination. The rGO film exhibits a



DOI: 10.1021/acsnano.7b01965
*ACS Nano* 2017, 11, 5087–5093

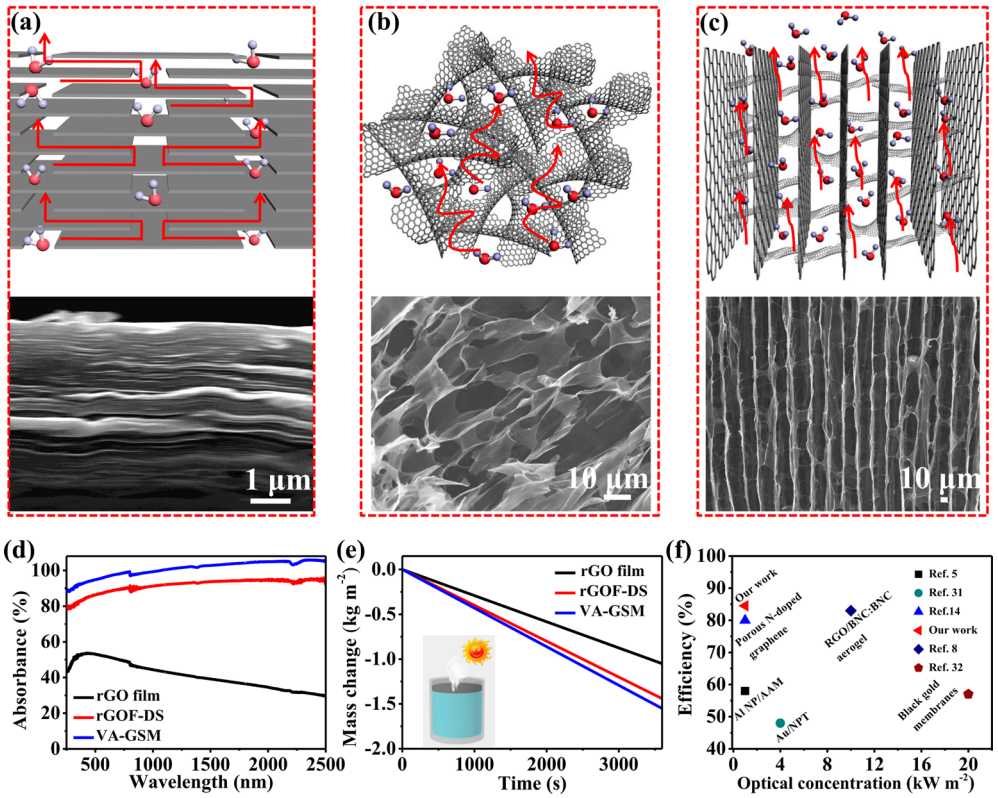


**Figure 2. Mechanism illustration of water transport channels with (a) rGO film, (b) rGOF-DS, and (c) VA-GSM for solar steam generation. (d) Absorbance spectra of rGO film, rGOF-DS, and VA-GSM in the wavelength range of 250−2500 nm. (e) Mass change of water with rGO film, rGOF-DS, and VA-GSM under 1 sun. Inset in (e) is the schematic illustration for solar steam generation using the simulated experimental setup. All experiments were conducted in the ambient temperature of 25 °C and the humidity of 22%. (f) Solar thermal conversion efficiency of VA-GSM compared with previous reports without the assistance of thermally insulating layer.**

tightly layer-by-layer assembled structure,[30] which severely hinders the diffusion of water molecules to the surface (Figures 2a and S8). The closed pores framework of rGOF-DS increases the transmission distance and diminishes subsequent evaporation (Figure 2b). In contrast, VA-GSM with highly vertically aligned graphene sheets provided the profitable open channels for water transport and vapor release (Figure 2c). Meanwhile, VA-GSM can absorb about 93% of the UV, 98% of visible, and nearly 100% of near-infrared solar irradiation, much higher than that of rGO film and rGOF-DS (Figure 2d). As a result, VA-GSM delivered the average water evaporation rate of 1.57 kg $m^{-2}$ (Figure 2e). The solar thermal conversion efficiency is up to 83.5% under only 1 sun, superior to most of the previous reports without the assistance of thermally insulating layer (Figure 2f and Table S1).[5,8,14,31,32] The open channels, high light absorption, and rapid water transport endow the VA-GSM with excellent photothermal transduction and timely water supply for efficient solar steam generation.

To further enhance the solar steam generation, we introduced a sandwich thermally insulating layer to the device (Figures 3a and S9a−d). After 60 min solar illumination of 1 sun, only about a 3.2 °C temperature change of water is observed (Figure 3b), much lower than that of the VA-GSM contact with water directly (Figure S9e−h). Meanwhile, the VA-GSM exhibits a thermal conductivity of 3.8 mW $m^{-1}$ $K^{-1}$, which is lower than most of the carbon materials at 298 K.[14] This minimized heat transfer to water induced by a thermally insulating layer and prevented thermal diffusion to the atmosphere caused by low thermal conductivity make a higher photothermal conversion efficiency. As a result, the average water evaporation rates are 1.62 and 6.25 kg $m^{-2}$ $h^{-1}$ under constant illuminations of 1 and 4 sun power with the assistance of thermally insulating layer (Figures 3c and S10). The values of water evaporation rates of VA-GSM are higher than other carbon materials such as graphene films (1 sun, 1.45 kg $m^{-2}$ $h^{-1}$),[13] carbon nanotubes (1 sun, 1.32 kg $m^{-2}$ $h^{-1}$),[33] and graphite (10 sun, 10.8 kg $m^{-2}$ $h^{-1}$)[34,35] (Figure 3f and Table S2). Moreover, the corresponding solar thermal conversion efficiencies are up to 86.5% and 94.2% under 1 and 4 sun, respectively. Under the solar illumination of 4 sun power, a stable surface temperature of VA-GSM floating on water at 73.5 °C is achieved in 5 min (Figures 3e and S11). These results confirm that hot localized solar thermal conversion was induced on the surface of VA-GSM, thus leading to a higher solar evaporation rate.

Solar energy is a sustainable and pollution-free source that can be used to solve many serious global challenges, and one of the most important is using solar energy for distillation to produce fresh water. As a promising material platform for efficient solar steam generation, VA-GSM can steadily produce clean water with an average rate of 6.22 kg $m^{-2}$ $h^{-1}$ under 4 sun irradiation from seawater (Bohai Sea), as shown in Figure 4a. The concentrations of five primary ions of $Na^+$, $Mg^{2+}$, $Ca^{2+}$, $K^+$, and $B^{3+}$ are significantly reduced with an ion rejection of 99.1% (Figure 4b,c). Meanwhile, the concentration of $Na^+$ ions is below the salinity levels defined by World Health Organization (WHO) and the standard of US Environmental Protection Agency (EPA).[36] VA-GSM can not only generate the clean



DOI: 10.1021/acsnano.7b01965
ACS Nano 2017, 11, 5087−5093

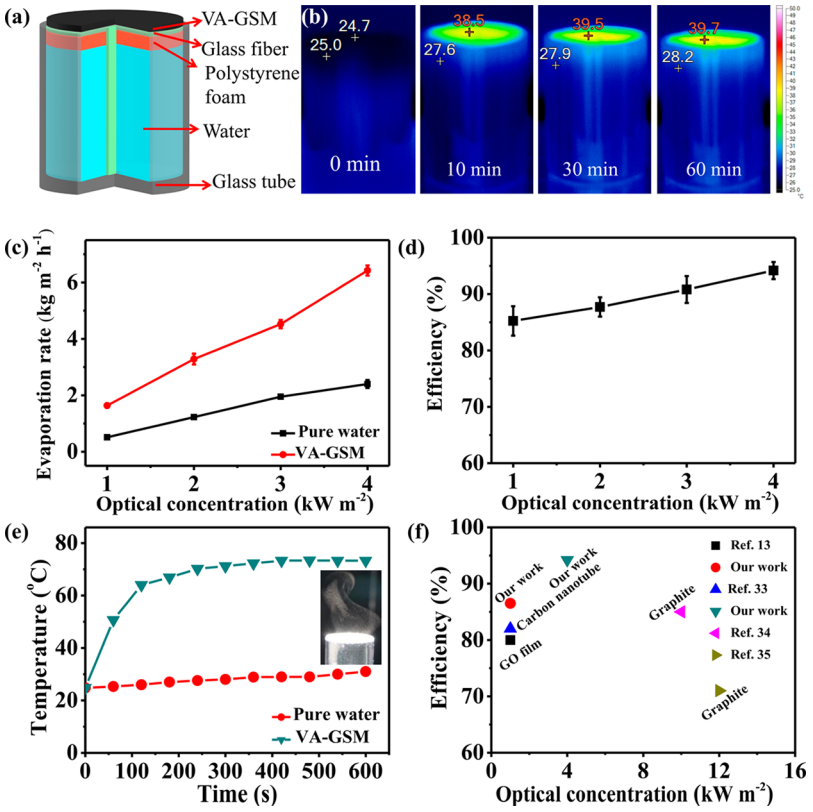


Figure 3. (a) Schematic illustration of solar steam generation with thermally insulating layer. The polystyrene foam serves to float the entire structure on water, and the hydrophilic and insulating glass fiber layer serves to deliver the water to the hot spot. (b) Temperatures of water under VA-GSM with thermally insulating layer after 60 min solar illumination of 1 sun. (c) The water mass change for pure water and VA-GSM under different optical concentration. (d) Solar thermal conversion efficiency of VA-GSM with different optical concentration calculated from (c), and the error bars in (c, d) indicate the standard deviation of the measurements. (e) Surface temperatures of pure water and VA-GSM under solar illumination of 4 sun as a function of irradiation time tested by an IR camera. Inset in (e) is the visible steam flow generated under 4 sun irradiation. (f) Solar steam efficiencies of VA-GSM compared to other reports with the assistance of thermally insulating layer.

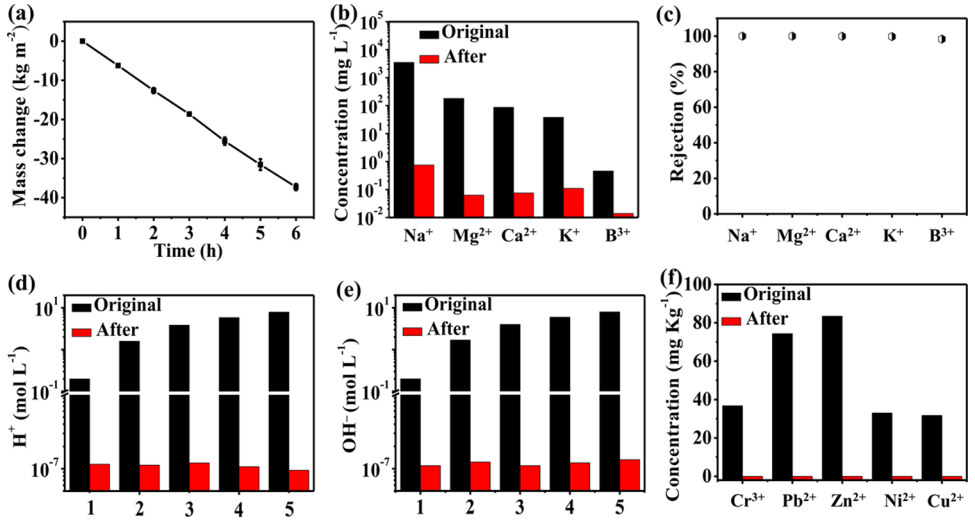


Figure 4. (a) Mass change of seawater *versus* time under solar illumination of 4 sun. (b) The measured concentrations of five primary ions in an actual seawater sample (Bohai Sea) before (original) and after solar thermal purification. (c) The ion rejection of seawater sample undergoing the solar thermal purification. (d) The concentration changes of $H^+$ in five acid solutions before (original) and after solar thermal purification. The samples with numbers 1−5 correspond to the original concentrations of $H^+$: 0.2, 2, 4, 6, 8 mol $mL^{-1}$, respectively. (e) The concentration changes of $OH^-$ in five alkali solutions before (original) and after solar thermal purification. The samples with numbers 1−5 correspond to the original concentrations of $OH^-$: 0.2, 2, 4, 6, 8 mol $mL^{-1}$, respectively. (f) Concentration changes of metal ions of $Cr^{3+}$, $Pb^{2+}$, $Zn^{2+}$, $Ni^{2+}$, and $Cu^{2+}$ in the simulated wastewater before (original) and after solar thermal purification.

water from seawater but also work well in rigorous conditions, such as strong acid and alkali solutions, and the average water evaporation rates are also measured with different water samples (Figure S12). As tested for the water containing the



DOI: 10.1021/acsnano.7b01965
ACS Nano 2017, 11, 5087−5093

high concentration of $H^+$ and $OH^-$ in the range of 0.2−8 mol $mL^{-1}$, the ion concentration of the sun thermally generated water is several orders of magnitude lower than that of the original samples, and the pH values of all the generated water are close to 7 with an ion rejection of 99.99% (Figures 4d,e and S13a,b). The heavy metal ions in drinking water can inactivate the proteins and enzymes in the human body and accumulate in human organs, causing chronic poisoning.[37,38] The purification of wastewater containing heavy metal ions is also well done on the basis of VA-GSM. As the example shown in Figure 4f, the concentrations of heavy metal ions such as $Cr^{3+}$, $Pb^{2+}$, $Zn^{2+}$, $Ni^{2+}$, and $Cu^{2+}$ are below 0.01 mg $kg^{-1}$ after purification with an ion rejection of 99.5% (Figure S13c), which is lower than the concentration defined by the drinking water standard (GB5749-2006). Compared with other technologies for water regeneration based on nanofiltration membranes,[39−43] reverse osmosis,[44−47] and electrodialysis,[48] solar steam generation of VA-GSM is much more efficient and lower in cost with a high rejection of ions, making it easy to scaled up for regeneration of clean water.

## CONCLUSION

In summary, VA-GSM with long-range vertically aligned graphene sheets has been developed by a scalable antifreeze-assisted freezing technique. The self-supporting VA-GSM possesses the run-through channels facilitating the water transport, high light absorption capacity for excellent photothermal transduction, and the extraordinary stability in rigorous conditions, ensuring the highly efficient solar thermal conversion for generation of clean water from seawater, common wastewater, and even concentrated acid and/or alkali solutions. VA-GSM has achieved the superb high efficiency of up to 86.5% under 1 sun and 94.2% under 4 sun illumination. Our results demonstrate the rational assembly of graphene into a structure-specialized architecture for the efficient utilization of solar energy for clean water, which is expected to be used for graphene-assisted solar steam generation to solve the issue of cleaning water by removing bacteria, oil, and other organic matter.

## EXPERIMENTAL SECTION

**Synthesis of GO.** GO suspension (7 mg $mL^{-1}$) was prepared from natural graphite powder according to a modified Hummers method as reported in our previous paper.[49,50] The GO sheets have lateral dimensions of 30−50 $\mu$m.

**Scalable Synthesis of VA-GSM.** The mixture of GO with ethanol (30:1, v/v) was transferred into a PTFE mold with a depth of several millimeters. Then the mold was placed on the surface of liquid nitrogen for 10 min for directional freeze casting from the bottom to the top. The sample can be produced in a large area by adjusting the sizes of the mold containers. Finally, VA-GSM was obtained by freeze-drying and annealing at 200 °C for 1 h and then treated at 1000 °C for 2 h under nitrogen atmosphere. For comparison, rGO samples with different amounts of additives (*e.g.*, ethanol and other organic solvents) were also prepared using the same conditions. All the samples were used with a thickness of 2 mm and treated with $O_2$-plasma unless otherwise noted.

**Synthesis of rGO Film.** Seven mL of GO (3 mg $mL^{-1}$) suspension was deposited onto a cellulose membrane filter to form a GO film through vacuum filtration, annealed at 200 °C for 1 h, and then treated at 1000 °C for 2 h under nitrogen atmosphere. The samples used for solar steam generation in the experiments were treated with $O_2$-plasma.

**Synthesis of rGOF-DS.** Three mL of GO (7 mg $mL^{-1}$) suspension was immersed into liquid nitrogen, followed by freeze-drying and annealing under the conditions identical to those used for preparation of VA-GSM. The samples had a thickness of 2 mm and were treated with $O_2$-plasma.

**Preparation of Concentrated Acid and Alkali Solutions and Pollutant Water.** Dense sulfuric acid ($H_2SO_4$) and sodium hydroxide (NaOH) solutions with different ion concentrations of $H^+$ and $OH^-$ (*ca.* 0.2, 2, 4, 6, and 8 mol $mL^{-1}$, respectively) were prepared by dissolving the solute in ultrapure water. The simulated wastewater with different heavy metal ions of $Cr^{3+}$, $Pb^{2+}$, $Zn^{2+}$, $Ni^{2+}$, and $Cu^{2+}$ was also prepared by dissolving chromic chloride, lead nitrate, zinc chloride, nickel chloride, and cupric nitrate in ultrapure water, respectively. The mass concentration is 100 mg $mL^{-1}$.

**Characterizations.** The samples morphology was investigated by SEM (JSM-7500F). The hydrophilic graphene surface was obtained by $O_2$-plasma treatment (65 W, 80 sccm, and 60 s). The absorbance spectra of VA-GSM were measured using a varian UV−vis spectrophotometer (Cary 5000), coupled with an Agilent integrating sphere. The temperature was measured using an IR camera (Fluke), and the water weight change through evaporation was measured using an electronic mass balance with an accuracy of 0.0001 g. The steam generation experiments were conducted in the lab using a solar simulator (CEL-HXF300) with an optical filter for the standard AM 1.5 G spectrum. The thermopile detector is smaller in area than the solar receiver, and the maximum-measured solar flux is regarded as the actual constant solar flux for the efficiency measurements. The ion concentrations of gathered water were measured by the inductively coupled plasma emission spectrometer (ICPE-9820, Shimadzu).

**Steam Generation Experiments.** The circular samples (24 mm in diameter) with different thicknesses were floated on water in a glass tube that was surrounded by thermally- insulating glass fibers. The samples were irradiated by a solar simulator under different optical concentrations, and the evaporation rates were measured for 60 min at steady-state condition. Both the weight loss and surface temperatures over the entire process were recorded using an electronic mass balance and IR camera, respectively.

**Estimation of Energy Conversion.** The energy conversion from solar illumination to thermal energy for steam generation was simply calculated from the evaporation amount of water.[5,32,35] The solar thermal conversion efficiency ($\eta$) is given by[5,13,14]

$$\eta = mh_{LV}/I$$

where $\eta$ is solar thermal conversion efficiency, $m$ is the evaporation rate, $h_{LV}$ is the total enthalpy of sensible heat (315 J $g^{-1}$, from *ca.* 25 to 100 °C with specific heat of 4.2 J $g\ K^{-1}$) and phase change of liquid to water (2256 J $g^{-1}$), and $I$ is the solar illumination energy.

In the calculation of efficiencies in our work, only the phase-change enthalpy is considered, and all the data in the figures are average values of several samples. The average evaporation rate of pure water in the dark conditions is subtracted from all the measured evaporation rates to eliminate the effect of natural water evaporation.

## ASSOCIATED CONTENT

### Supporting Information

The Supporting Information is available free of charge on the ACS Publications website at DOI: 10.1021/acsnano.7b01965.

SEM images of rGO samples prepared with different additives, freezing direction, and amount of ethanol are characterized. The stress−strain curves, BET and CA of VA-GSM, including details of steam generation experiments with VA-GSM are measured. (PDF)

The VA-GSM can be cut easily (AVI)

## AUTHOR INFORMATION

### Corresponding Author

*E-mail: lqu@bit.edu.cn.

### ORCID

Liangti Qu: 0000-0002-7320-2071



DOI: 10.1021/acsnano.7b01965
*ACS Nano* 2017, 11, 5087−5093

### Author Contributions

P.P. Zhang and J. Li contributed equally to the work.

### Notes

The authors declare no competing financial interest.

## ACKNOWLEDGMENTS

This work was supported by NSFC (nos. 21325415 and 51673026), Beijing Natural Science Foundation (2152028), Beijing Municipal Science and Technology Commission (Z161100002116022), and 111 Project 807012.

## REFERENCES

(1) Politano, A.; Argurio, P.; Di Profio, G.; Sanna, V.; Cupolillo, A.; Chakraborty, S.; Arafat, H. A.; Curcio, E. Photothermal Membrane Distillation for Seawater Desalination. *Adv. Mater.* **2017**, *29*, 1603504.

(2) Yang, H. C.; Hou, J. W.; Chen, V.; Xu, Z. K. Janus Membranes: Exploring Duality for Advanced Separation. *Angew. Chem., Int. Ed.* **2016**, *55*, 13398−13407.

(3) Fane, A. G.; Wang, R.; Hu, M. X. Synthetic Membranes for Water Purification: Status and Future. *Angew. Chem., Int. Ed.* **2015**, *54*, 3368−3386.

(4) Fujiwara, M.; Imura, T. Photo Induced Membrane Separation for Water Purification and Desalination Using Azobenzene Modified Anodized Alumina Membranes. *ACS Nano* **2015**, *9*, 5705−5712.

(5) Zhou, L.; Tan, Y. L.; Wang, J. Y.; Xu, W. C.; Yuan, Y.; Cai, W. S.; Zhu, S. N.; Zhu, J. 3D Self-Assembly of Aluminium Nanoparticles for Plasmon-Enhanced Solar Desalination. *Nat. Photonics* **2016**, *10*, 393−398.

(6) Zhang, L. B.; Tang, B.; Wu, J. B.; Li, R. Y.; Wang, P. Hydrophobic Light-to-Heat Conversion Membranes with Self-Healing Ability for Interfacial Solar Heating. *Adv. Mater.* **2015**, *27*, 4889−4894.

(7) Liu, Y. M.; Yu, S. T.; Feng, R.; Bernard, A.; Liu, Y.; Zhang, Y.; Duan, H. Z.; Shang, W.; Tao, P.; Song, C. Y.; Deng, T. A Bioinspired, Reusable, Paper-Based System for High-Performance Large-Scale Evaporation. *Adv. Mater.* **2015**, *27*, 2768−2774.

(8) Jiang, Q. S.; Tian, L. M.; Liu, K. K.; Tadepalli, S.; Raliya, R.; Biswas, P.; Naik, R. R.; Singamaneni, S. Bilayered Biofoam for Highly Efficient Solar Steam Generation. *Adv. Mater.* **2016**, *28*, 9400−9407.

(9) Wang, X. P.; Lv, L. X.; Cheng, Z. H.; Gao, J.; Dong, L. Y.; Hu, C. G.; Qu, L. T. High-Density Monolith of N-Doped Holey Graphene for Ultrahigh Volumetric Capacity of Li-Ion Batteries. *Adv. Energy Mater.* **2016**, *6*, 1502100.

(10) Zhao, Y.; Hu, C. G.; Song, L.; Wang, L. X.; Shi, G. Q.; Dai, L. M.; Qu, L. T. Functional Graphene Nanomesh Foam. *Energy Environ. Sci.* **2014**, *7*, 1913−1918.

(11) Zhao, Y.; Hu, C. G.; Hu, Y.; Cheng, H. H.; Shi, G. Q.; Qu, L. T. A Versatile, Ultralight, Nitrogen-Doped Graphene Framework. *Angew. Chem.* **2012**, *124*, 11533−11537.

(12) Hu, C. G.; Xue, J. L.; Dong, L. Y.; Jiang, Y.; Wang, X. P.; Qu, L. T.; Dai, L. M. Scalable Preparation of Multifunctional Fire-Retardant Ultralight Graphene Foams. *ACS Nano* **2016**, *10*, 1325−1332.

(13) Li, X. Q.; Xu, W. C.; Tang, M. Y.; Zhou, L.; Zhu, B.; Zhu, S. N.; Zhu, J. Graphene Oxide-Based Efficient and Scalable Solar Desalination under One Sun with a Confined 2D Water Path. *Proc. Natl. Acad. Sci. U. S. A.* **2016**, *113*, 13953−13958.

(14) Ito, Y.; Tanabe, Y.; Han, J. H.; Fujita, T.; Tanigaki, K.; Chen, M. W. Multifunctional Porous Graphene for High-Efficiency Steam Generation by Heat Localization. *Adv. Mater.* **2015**, *27*, 4302−4307.

(15) Xu, Z.; Liu, Y. J.; Zhao, X. L.; Peng, L.; Sun, H. Y.; Xu, Y.; Ren, X. B.; Jin, C. H.; Xu, P.; Wang, M.; Gao, C. Ultrastiff and Strong Graphene Fibers *via* Full-Scale Synergetic Defect Engineering. *Adv. Mater.* **2016**, *28*, 6449−6456.

(16) Lv, L. X.; Zhang, P. P.; Cheng, H. H.; Zhao, Y.; Zhang, Z. P.; Shi, G. Q.; Qu, L. T. Solution-Processed Ultraelastic and Strong Air-Bubbled Graphene Foams. *Small* **2016**, *12*, 3229−3234.

(17) Wu, Y. P.; Yi, N. B.; Huang, L.; Zhang, T. F.; Fang, S. L.; Chang, H. C.; Li, N.; Oh, J. Y.; Lee, J. A.; Kozlov, M.; Chipara, A. C.; Terrones, H.; Xiao, P. S.; Long, G. K.; Huang, Y.; Zhang, F.; Zhang, L.; Lepró, X.; Haines, C.; Lima, M. D.; et al. Three-Dimensionally Bonded Spongy Graphene Material with Super Compressive Elasticity and Near-Zero Poisson's Ratio. *Nat. Commun.* **2015**, *6*, 6141−6149.

(18) Zhao, X. L.; Xu, Z.; Zheng, B. N.; Gao, C. Macroscopic Assembled, Ultrastrong and $H_2SO_4$-Resistant Fibres of Polymer-Grafted Graphene Oxide. *Sci. Rep.* **2013**, *3*, 3164−3170.

(19) Fan, X. B.; Peng, W. C.; Li, Y.; Li, X. Y.; Wang, S. L.; Zhang, G. L.; Zhang, F. B. Deoxygenation of Exfoliated Graphite Oxide under Alkaline Conditions: a Green Route to Graphene Preparation. *Adv. Mater.* **2008**, *20*, 4490−4493.

(20) Raymond, J. A.; DeVries, A. L. Adsorption Inhibition as a Mechanism of Freezing Resistance in Polar Fishes. *Proc. Natl. Acad. Sci. U. S. A.* **1977**, *74*, 2589−2593.

(21) Geng, H. Y.; Liu, X.; Shi, G. S.; Bai, G. Y.; Ma, J.; Chen, J. B.; Wu, Z. Y.; Song, Y. L.; Fang, H. P.; Wang, J. J. Graphene Oxide Restricts Growth and Recrystallization of Ice Crystals. *Angew. Chem., Int. Ed.* **2017**, *56*, 997−1001.

(22) Qiu, L.; Liu, J. Z.; Chang, S. L. Y.; Wu, Y. Z.; Li, D. Biomimetic Superelastic Graphene-Based Cellular Monoliths. *Nat. Commun.* **2012**, *3*, 1241−1247.

(23) Xu, Y. X.; Sheng, K. X.; Li, C.; Shi, G. Q. Self-Assembled Graphene Hydrogel *via* a One-Step Hydrothermal Process. *ACS Nano* **2010**, *4*, 4324−4330.

(24) Xu, Y. X.; Wu, Q.; Sun, Y. Q.; Bai, H.; Shi, G. Q. Three-Dimensional Self-Assembly of Graphene Oxide and DNA into Multifunctional Hydrogels. *ACS Nano* **2010**, *4*, 7358−7362.

(25) Zhao, F.; Wang, L. X.; Zhao, Y.; Qu, L. T.; Dai, L. M. Graphene Oxide Nanoribbon Assembly toward Moisture-Powered Information Storage. *Adv. Mater.* **2017**, *29*, 1604972.

(26) Yao, B. W.; Chen, J.; Huang, L.; Zhou, Q. Q.; Shi, G. Q. Base-Induced Liquid Crystals of Graphene Oxide for Preparing Elastic Graphene Foams with Long-Range Ordered Microstructures. *Adv. Mater.* **2016**, *28*, 1623−1629.

(27) Zhao, J. P.; Yang, B. J.; Zheng, Z. M.; Yang, J.; Yang, Z.; Zhang, P.; Ren, W. C.; Yan, X. B. Facile Preparation of One-Dimensional Wrapping Structure: Graphene Nanoscroll-Wrapped of $Fe_3O_4$ Nanoparticles and Its Application for Lithium-Ion Battery. *ACS Appl. Mater. Interfaces* **2014**, *6*, 9890−9896.

(28) Zhao, J. P.; Yang, B. J.; Yang, Z.; Zhang, P.; Zheng, Z. M.; Ren, W. C.; Yan, X. B. Facile Preparation of Large-Scale Graphene Nanoscrolls from Graphene Oxide Sheets by Cold Quenching in Liquid Nitrogen. *Carbon* **2014**, *79*, 470−477.

(29) Yu, S. T.; Zhang, Y.; Duan, H. Z.; Liu, Y. M.; Quan, X. J.; Tao, P.; Shang, W.; Wu, J. B.; Song, C. Y.; Deng, T. The Impact of Surface Chemistry on the Performance of Localized Solar-Driven Evaporation System. *Sci. Rep.* **2015**, *5*, 13600−13609.

(30) Dong, L. Y.; Hu, C. G.; Song, L.; Huang, X. K.; Chen, N.; Qu, L. T. A Large-Area, Flexible, and Flame-Retardant Graphene Paper. *Adv. Funct. Mater.* **2016**, *26*, 1470−1476.

(31) Zhou, L.; Zhuang, S. D.; He, C. Y.; Tan, Y. L.; Wang, Z. L.; Zhu, J. Self-Assembled Spectrum Selective Plasmonic Absorbers with Tunable Bandwidth for Solar Energy Conversion. *Nano Energy* **2017**, *32*, 195−200.

(32) Bae, K.; Kang, G. M.; Cho, S. K.; Park, W.; Kim, K.; Padilla, W. J. Flexible Thin-Film Black Gold Membranes with Ultrabroadband Plasmonic Nanofocusing for Efficient Solar Vapour Generation. *Nat. Commun.* **2015**, *6*, 10103−10111.

(33) Wang, Y. C.; Zhang, L. B.; Wang, P. Self-Floating Carbon Nanotube Membrane on Macroporous Silica Substrate for Highly Efficient Solar-Driven Interfacial Water Evaporation. *ACS Sustainable Chem. Eng.* **2016**, *4*, 1223−1230.

(34) Ghasemi, H.; Ni, G.; Marconnet, A. M.; Loomis, J.; Yerci, S.; Miljkovic, N.; Chen, G. Solar Steam Generation by Heat Localization. *Nat. Commun.* **2014**, *5*, 4449−4455.

(35) Ni, G.; Li, G.; Boriskina, S. V.; Li, H. X.; Yang, W. L.; Zhang, T. J.; Chen, G. Steam Generation under One Sun Enabled by a Floating Structure with Thermal Concentration. *Nat. Energy* **2016**, *1*, 16126−16132.



DOI: 10.1021/acsnano.7b01965
*ACS Nano* 2017, 11, 5087−5093

(36) Smith, A. H.; Lopipero, P. A.; Bates, M. N.; Steinmaus, C. M. Arsenic Epidemiology and Drinking Water Standards. *Science* **2002**, *296*, 2145−2146.
(37) Kneer, R.; Zenk, M. H. Phytochelatins Protect Plant Enzymes from Heavy Metal Poisoning. *Phytochemistry* **1992**, *31*, 2663−2667.
(38) Schützendübel, A.; Polle, A. Plant Responses to Abiotic Stresses: Heavy Metal-Induced Oxidative Stress and Protection by Mycorrhization. *J. Exp. Bot.* **2002**, *53*, 1351−1365.
(39) Childress, A. E.; Elimelech, M. Relating Nanofiltration Membrane Performance to Membrane Charge (Electrokinetic) Characteristics. *Environ. Sci. Technol.* **2000**, *34*, 3710−3716.
(40) Levenstein, R.; Hasson, D.; Semiat, R. Utilization of the Donnan Effect for Improving Electrolyte Separation with Nanofiltration Membranes. *J. Membr. Sci.* **1996**, *116*, 77−92.
(41) Mohammad, A. W.; Othaman, R.; Hilal, N. Potential Use of Nanofiltration Membranes in Treatment of Industrial Wastewater from Ni-P Electroless Plating. *Desalination* **2004**, *168*, 241−252.
(42) Han, Y.; Xu, Z.; Gao, C. Ultrathin Graphene Nanofiltration Membrane for Water Purification. *Adv. Funct. Mater.* **2013**, *23*, 3693−3700.
(43) Hu, M.; Mi, B. X. Enabling Graphene Oxide Nanosheets as Water Separation Membranes. *Environ. Sci. Technol.* **2013**, *47*, 3715−3723.
(44) Jin, W. Q.; Toutianoush, A.; Tieke, B. Use of Polyelectrolyte Layer-by-Layer Assemblies as Nanofiltration and Reverse Osmosis Membranes. *Langmuir* **2003**, *19*, 2550−2553.
(45) Hyung, H.; Kim, J. H. A Mechanistic Study on Boron Rejection by Sea Water Reverse Osmosis Membranes. *J. Membr. Sci.* **2006**, *286*, 269−278.
(46) Gu, J. E.; Lee, S.; Stafford, C. M.; Lee, J. S.; Choi, W.; Kim, B. Y.; Baek, K. Y.; Chan, E. P.; Chung, J. Y.; Bang, J.; Lee, J. H. Molecular Layer-by-Layer Assembled Thin-Film Composite Membranes for Water Desalination. *Adv. Mater.* **2013**, *25*, 4778−4782.
(47) Cho, K. L.; Hill, A. J.; Caruso, F.; Kentish, S. E. Chlorine Resistant Glutaraldehyde Crosslinked Polyelectrolyte Multilayer Membranes for Desalination. *Adv. Mater.* **2015**, *27*, 2791−2796.
(48) Sun, P. Z.; Wang, K. L.; Zhu, H. W. Recent Developments in Graphene-Based Membranes: Structure, Mass-Transport Mechanism and Potential Applications. *Adv. Mater.* **2016**, *28*, 2287−2310.
(49) Zhao, F.; Cheng, H. H.; Zhang, Z. P.; Jiang, L.; Qu, L. T. Direct Power Generation from a Graphene Oxide Film under Moisture. *Adv. Mater.* **2015**, *27*, 4351−4357.
(50) Cheng, H. H.; Hu, Y.; Zhao, F.; Dong, Z. L.; Wang, Y. H.; Chen, N.; Zhang, Z. P.; Qu, L. T. Moisture-Activated Torsional Graphene-Fiber Motor. *Adv. Mater.* **2014**, *26*, 2909−2913.



DOI: 10.1021/acsnano.7b01965
*ACS Nano* 2017, 11, 5087−5093